HHS Public Access

Author manuscript

Curr Biol. Author manuscript; available in PMC 2021 September 07.

Published in final edited form as:

Curr Biol. 2020 September 07; 30(17): 3293–3303.e4. doi:10.1016/j.cub.2020.06.017.

Parietal cortex is required for the integration of acoustic evidence

Justin D. Yao[*,1], **Justin Gimoto**[1], **Christine M. Constantinople**[1,4], **Dan H. Sanes**[1,2,3,4]

[1]Center for Neural Science, New York University, New York, NY 10003

[2]Department of Psychology, New York University, New York, NY 10003

[3]Department of Biology, New York University, New York, NY 10003

[4]Neuroscience Institute, NYU Langone Medical Center, New York University, New York, NY 10003

SUMMARY

Sensory-driven decisions are formed by accumulating information over time. While parietal cortex activity is thought to represent accumulated evidence for sensory-based decisions, recent perturbation studies in rodents and non-human primates have challenged the hypothesis that these representations actually influence behavior. Here, we asked whether the parietal cortex integrates acoustic features from auditory cortical inputs during a perceptual decision-making task. If so, we predicted that selective inactivation of this projection should impair subjects' ability to accumulate sensory evidence. We trained gerbils to perform an auditory discrimination task and obtained measures of integration time as a readout of evidence accumulation capability. Minimum integration time was calculated behaviorally as the shortest stimulus duration for which subjects could discriminate the acoustic signals. Direct pharmacological inactivation of parietal cortex increased minimum integration times, suggesting its role in the behavior. To determine the specific impact of sensory evidence, we chemogenetically inactivated the excitatory projections from auditory cortex to parietal cortex, and found this was sufficient to increase minimum behavioral integration times. Our signal detection theory based model accurately replicated behavioral outcomes, and indicated that the deficits in task performance were plausibly explained by elevated sensory noise. Together, our findings provide causal evidence that parietal cortex plays a role in the network that integrates auditory features for perceptual judgments.

[*]**Lead Contact** Justin D. Yao, Center for Neural Science, New York University, 4 Washington Place, Room 621, New York, NY 10003, jdyao@nyu.edu.

Author Contributions

Conceptualization, J.D.Y. and D.H.S.; Methodology, J.D.Y. and D.H.S.; Investigation, J.D.Y. and J.G; Formal Analysis, J.D.Y. and C.M.C.; Visualization, J.D.Y. and D.H.S.; Writing – Original Draft, J.D.Y. and D.H.S.; Writing – Review & Editing, J.D.Y., C.M.C., and D.H.S. Funding Acquisition, J.D.Y. and D.H.S.

Declaration of interest

The authors whose names are listed immediately above certify that they have no affiliations with or involvement in any organization or entity with any financial, or non-financial interest in the subject matter or materials discussed in this manuscript. The authors declare no competing interests.

Keywords

auditory cortex; parietal cortex; auditory perception; temporal integration; accumulation of evidence; decision-making

INTRODUCTION

Representations of environmental signals are transformed along ascending sensory pathways. A principal characteristic of this transformation is that sensory information is encoded over an increasing time span in higher cortical regions [1–3]. For example, secondary auditory cortex neurons integrate time-varying acoustic information over a longer duration than observed in primary auditory cortex neurons [4–6]. These longer integration times correlate with the duration of perceptually meaningful attributes such as phonemes and words [7,8]. Overall, perceptual judgements emerge from the temporal integration of sensory inputs downstream of primary sensory cortices [9]. Furthermore, the accuracy of such perception can be increased by reducing sensory noise during the temporal integration process [10, 11].

The parietal cortex is thought to integrate sensory evidence relayed from sensory cortices, thereby supporting perceptual decisions [12–16]. Recent work has also shown that parietal cortex plays a causal role in decision-making [17]. Parietal cortex neurons receive input from primary and secondary areas of sensory cortices [18–27], and are strongly modulated by behavioral relevance and context [12–14, 16, 24, 28–31]. However, the extent to which the parietal cortex is causally involved in the accumulation of sensory evidence remains uncertain. Microstimulation of the primate lateral intraparietal cortex during accumulation of visual evidence biased animals' performance [32], yet pharmacological inactivation produced no effect [33]. Furthermore, pharmacological inactivation of parietal cortex in rats trained to accumulate auditory clicks has so far failed to produce appreciable effects on behavioral performance [15, 31], even though posterior parietal cortex inactivation can impair rats' ability to accumulate visual evidence [31] (see [34] for detailed discussion).

Here, we trained gerbils to accumulate sensory evidence using auditory stimuli that contain envelope information, a feature that is present in all natural sounds, including human speech [35–37]. Envelope information is generally studied with periodic amplitude modulated (AM) stimuli, and longer AM durations are associated with superior performance on detection and discrimination tasks [38–42]. In contrast, previous accumulation of evidence studies in rodents have used auditory stimuli (clicks) that do not contain energy in the natural AM range [43], and therefore may not engage cortical pathways in the same way as stimuli with more naturalistic acoustic features. To address these issues, animals were trained to perform an AM rate discrimination task, and we assessed evidence accumulation behaviorally as the shortest stimulus duration for which animals accurately performed the task. This behavioral measure of integration time is distinct from an integration time constant. We then pharmacologically inactivated auditory-recipient parietal cortex, chemogenetically inactivated the auditory cortex projection to parietal cortex, and tested whether animals' ability to accumulate acoustic information was degraded. Direct pharmacological

inactivation of parietal cortex increased minimum behavioral integration times, suggesting its role in behavioral performance. Chemogenetic inactivation of the excitatory projections from auditory cortex to parietal cortex was sufficient to increase minimum behavioral integration times, demonstrating the direct impact of reducing sensory evidence. Our signal detection theory based model replicated behavioral outcomes and suggested that the deficits in task performance could be attributed to elevated sensory noise during evidence accumulation. Overall, our results provide causal evidence that the parietal cortex plays a role in the network that integrates auditory features for perceptual decisions.

RESULTS

Task performance scales with stimulus duration

Adult gerbils were trained to perform a single-interval, two-alternative forced-choice (2AFC) amplitude-modulation (AM) rate discrimination task. Gerbils self-initiated each trial by placing their nose in a cylindrical port for a minimum of 100 msec. A food pellet reward was delivered when they approached the left food tray following a 4 Hz AM signal, or the right food tray following a 10 Hz AM signal (Figure 1A). Task performance was recorded across a range of AM stimulus durations (100–2000 ms) that varied randomly on each trial. Each animal's task performance was assessed across 3 sessions. Figure S1A displays psychometric functions from 3 animals across 3 test sessions. Minimum integration times were calculated for each subject as the stimulus duration corresponding to a proportion correct of 0.76, which is equivalent to the signal detection metric, *d'*, equal to 1 [44, 45]. For all animals (n = 17), performance across all 3 test sessions remained stable as minimum integration times did not change significantly (Figure S1B; one-way repeated measures ANOVA; $F_{(2,32)} = 0.28$, $p = 0.76$). Figure 1B displays average psychometric functions from each animal tested, along with the population mean and standard error. Task performance improved with increasing stimulus duration (one-way repeated measures ANOVA; $F_{(4,64)} = 317.9$, $p < 0.0001$). Specifically, performance was slightly above chance for stimulus durations of < 300 ms, and reached a maximum at ≥ 800 ms. The proportion of correct trials significantly increased with stimulus duration (two-way mixed model ANOVA; $F_{(1,16)} = 25009.9$, $p < 0.0001$), but there was no significant difference between 4 versus 10 Hz trials (two-way mixed model ANOVA; $F_{(1,16)} = 2.91$, $p = 0.11$), nor was there an interaction between proportion of correct trials and trial type (two-way mixed model ANOVA; $F_{(4,64)} = 0.93$, $p = 0.45$), demonstrating animals were not biased to either stimuli. The distributions of average minimum integration time across trial types are plotted in Figure 1C. Average minimum integration times were similar across the trial types (one-way repeated measures ANOVA; $F_{(2,32)} = 2.49$, $p = 0.10$), further demonstrating no difference in task performance between 4 and 10 Hz trials. Across all subjects, an average stimulus duration of 355 ± 24 ms was required to discriminate the two AM rates at the criterion of 0.76 proportion correct. Thus, temporal integration can be accurately measured with this approach, permitting us to assess the underlying mechanisms.

Location of auditory cortex recipient parietal cortex

To perform selective manipulations of auditory cortex-recipient parietal cortex, we first conducted a set of anatomical experiments to identify the appropriate location (n = 9). We

targeted auditory cortex, as well as secondary dorsal auditory cortex, as candidate projection areas since parietal cortex receives direct and indirect input from primary and secondary cortices [25]. Injection sites were made 300 and 800 μm below the cortical surface, targeting layers 2/3 and 5, respectively. As shown in Figure 2A and B, an anterograde vector (AAV-hSyn-TurboRFP) was injected into auditory cortex, resulting in a direct projection to both secondary dorsal auditory cortex (Figure 2D) and the parietal cortex (Figure 2E, F) (n = 2). Anterograde labeling in parietal cortex was identified across 18–24 50 μm sections, suggesting that auditory cortex recipient labeling into parietal cortex spanned ~900–1200 μm across the rostrocaudal axis. Across the mediolateral axis, anterograde labeling in parietal cortex spanned ~800–1000 μm. Based in the gerbil atlas [46], these coordinates span their designated “medial parietal association cortex”. We also injected a different anterograde vector (AAV-hSyn-EGFP) into secondary dorsal auditory cortex, and demonstrated a direct projection to parietal cortex (Figure 2G, H, and I) (n = 3). To confirm these findings, we injected a retrograde vector (AAVrg-hSyn-EGFP) into parietal cortex (Figure 2J, K), and identified retrogradely labeled cell bodies within secondary dorsal auditory cortex (Figure 2L) and auditory cortex (Figure 2M) (n = 4). Auditory cortex and secondary dorsal auditory cortex terminals within parietal cortex typically spanned most of the cortical depth, with the majority of labeled axons encompassing superficial (~200–300 μm) and deep (~800 μm) layers. Together, these experiments confirmed a rich projection from primary and secondary auditory cortices to parietal cortex, and established the anatomical location to conduct loss-of-function experiments.

Inactivation of parietal cortex impairs auditory task performance

We next sought to determine whether parietal cortex activity was necessary for performance on the auditory discrimination task. To do so, we reversibly silenced auditory cortex-recipient parietal cortex with bilateral local infusions of muscimol, a selective gamma-aminobutryic acid class A receptor ($GABA_AR$) agonist. As illustrated in Figure 3A, cannulae were implanted bilaterally over the parietal cortex of well-trained animals. Following one week of recovery and return of good performance (see STAR METHODS), either muscimol or saline were locally infused on alternate days, and animals were tested on the auditory temporal integration task. Each animal (n = 7) was tested across 3 sessions of muscimol infusion and 3 sessions of saline infusion. Figure 3B displays average task performance for each animal during infusion sessions of muscimol (thin orange lines) and saline (thin blue lines), along with the group averages and standard errors (thick lines and shading). When comparing task performance between infusion groups, we found a significant main effect of infusion group (two-way mixed model ANOVA; $F_{(1,6)} = 22.4$, $p = 0.003$), and post-hoc analyses revealed significant differences in performance between infusion groups for all stimulus durations except the shortest duration of 100 ms and 800 ms (two-tailed t-tests; Holm-Bonferroni-corrected; 300 ms: $p = 0.0009$, $t = 5.14$; 600 ms: $p < 0.0001$, $t = 8.32$; 1000 ms: $p = 0.017$, $t = 3.16$; 2000 ms: $p = 0.03$, $t = 2.76$). As shown in Figure 3C, average minimum integration times displayed a significant difference across infusion groups and the no infusion condition (one-way repeated measures ANOVA; $F_{(2,12)} = 10.13$, $p = 0.003$). A post-hoc analysis indicated muscimol infusion sessions yielded significantly longer integration times compared to no infusion and saline sessions (two-tailed t-tests; Holm-Bonferroni-corrected; no infusion: $p = 0.023$, $t = -3.01$; saline: p =

0.013, t = −3.48). A similar effect was observed for both 4 Hz- and 10 Hz trials (Figure S2A, B). Psychometric slopes were similar across infusion groups (one-way repeated measures ANOVA; F(2,12) = 2.65, p = 0.11). To determine whether task performance changed across test sessions, we compared minimum integration time across muscimol infusion session order and found no difference across test session days (one-way repeated measures ANOVA; F(2,12) = 0.68, p = 0.52).

For assigned incorrect trials, animals would either approach the wrong reward port or not approach either food tray (“no response”) within 5 sec of stimulus presentation (see STAR METHODS). We found no difference in the proportion of “no response” incorrect trials across infusion groups and the no infusion condition (one-way repeated measures ANOVA; F(2,12) = 2.89, p = 0.09). To determine whether muscimol affected non-sensory task factors such as motor function, or induced a generalized spatial deficit, we compared response latencies between saline and muscimol sessions as a function of stimulus duration, and found no main effect of infusion group (two-way mixed model ANOVA; $F_{(1,6)} = 0.34$, p = 0.58; Figure S2C). Furthermore, we compared the number of right versus left choices on the longest stimulus durations and found no difference for the muscimol group (two-tailed t-test: p = 0.30, t = 1.08). To determine whether muscimol influenced overall spatial processing during task performance, we compared the difference for right versus left choices between saline and muscimol conditions. A two-tailed t-test demonstrated no difference between saline versus muscimol conditions (two-tailed t-test: p = 0.72, t = 0.36) suggesting parietal cortex inactivation with muscimol did not produce a generalized spatial deficit. In addition, the number of trials for each animal were similar between infusion groups (two-tailed t-test; saline = 173 ± 9; muscimol = 174 ± 19; p = 0.94, t = 0.08). Thus, the animals performed the task similarly during each condition. These results suggest that inactivating parietal cortex with muscimol impairs performance on a 2AFC auditory discrimination task, and also increases integration time.

Inactivation of auditory cortex afferents to parietal cortex increases auditory integration time

Inactivation of parietal cortex resulted in diminished performance which could be attributable to factors other than integration of auditory input. To assess the contribution of auditory cortex projections to parietal cortex on behavioral integration time, we used a chemogenetic approach to selectively and reversibly inactivate auditory cortex excitatory inputs to the parietal cortex. We first bilaterally injected an adenovirus containing a CamKII promotor that transfects pyramidal neurons with HM4Di, an inhibitory DREADD receptor, into auditory cortex of well-trained gerbils. We then bilaterally implanted cannulae over parietal cortex for local infusion of a chemogenetic actuator of HM4D (compound 21, C21) or saline (Figure 4A). Following a ~3-week period to permit adequate viral expression, animals were tested in a manner similar to muscimol experiments. Specifically, each animal (n = 5) was tested across alternating sessions of C21 (3 sessions) and saline infusions (3 sessions). When behavioral testing was completed, we confirmed the presence of HM4Di-mCherry-infected auditory cortex neurons (Figure 4B, C), and also confirmed that auditory cortex terminals were labeled within parietal cortex (Figure 4D). Figure 4E displays average task performance for each animal during infusion sessions of C21 (thin purple lines) and

saline (thin blue lines), along with the group averages and standard errors (thick lines and shading). When comparing task performance between infusion groups, we found a significant main effect of infusion group (two-way mixed model ANOVA; $F_{(1,4)} = 86.8$, $p = 0.0007$), and post-hoc analyses revealed significant differences in performance between infusion groups for the three stimulus durations that determined integration time (two-tailed t-tests; Holm-Bonferroni-corrected; 300 ms: $p = 0.0005$; $t = 5.56$; 600 ms: $p = 0.0006$; $t = 7.58$; 800 ms $p = 0.023$; $t = 3.04$). Therefore, there were no differences in asymptotic performance at durations of 1000 and 2000 ms. As shown in Figure 4F, average minimum integration times for each animal displayed a significant difference across infusion groups (one-way repeated measures ANOVA; $F_{(2,8)} = 25.12$, $p = 0.0004$). A post-hoc analysis indicated that C21 infusion caused significantly greater integration times compared to the no infusion and saline sessions (two-tailed t-tests; Holm-Bonferroni-corrected; no infusion: $p = 0.005$, $t = -5.61$; saline: ($p = 0.0027$, $t = -6.65$). A similar effect was observed for both 4 Hz- and 10 Hz trials (Figure S3A, B). Psychometric slopes were similar across infusion groups and the no infusion condition (one-way repeated measures ANOVA; $F(2,8) = 3.94$, $p = 0.06$). To determine whether task performance changed across test sessions, we compared minimum integration time across C21 infusion session order and found no difference across test session days (one-way repeated measures ANOVA; $F(2,8) = 0.19$, $p = 0.83$). We compared response latencies between saline and C21 sessions as a function of stimulus duration and found no main effect of infusion group (two-way mixed model ANOVA; $F_{(1,4)} = 0.0006$, $p = 0.98$; Figure S3C), suggesting C21 did not impair motor function as the animals performed the task similarly during each condition. The results suggest that chemogenetically perturbing excitatory auditory cortex inputs into parietal cortex significantly increases auditory integration times without affecting asymptotic performance.

For assigned incorrect trials, animals would either approach the wrong reward port or not approach either food tray (“no response”) within 5 sec of stimulus presentation (see STAR METHODS). We found no difference in the proportion of “no response” incorrect trials across infusion groups and the no infusion condition (one-way repeated measures ANOVA; $F(2,8) = 0.14$, $p = 0.87$). To determine whether muscimol or C21 manipulations differentially affected the proportion of “no response” incorrect trials, we compared the difference in the proportion of “no response” incorrect trials across Saline versus Muscimol and Saline versus C21 infusion sessions and found no difference between infusion manipulations (Wilcoxon rank sum test, $p = 0.88$). This suggests that the proportion of “no response” incorrect trials were not differentially affected by the inactivation manipulations.

One alternative explanation for our findings is that C21 has a direct effect on neural activity. To test this, we infused C21 into bilateral parietal cortex of well-trained gerbils ($n = 3$) that did not receive bilateral HM4Di-mCherry injections into auditory cortex (Figure S4A). We found no significant interaction between infusion group and task performance between saline and C21 infusion sessions (3 sessions each) (two-way mixed model ANOVA; $F_{(1,2)} = 15.5$, $p = 0.06$). Another alternative explanation for our findings is that perturbing excitatory auditory cortex input into parietal cortex reduces auditory sensation similar to lowering sound level and decreasing overall firing rate. Individual auditory cortex cells can display changes in firing rate across sound level, however, as a population auditory cortex displays a lognormal distribution of firing rate across a broad range of stimulus conditions [47]. Thus,

we expected no difference in behavioral performance across sound level. We confirmed this by finding no difference in task performance between two sound levels of 50 versus 66 dB SPL (n = 3 gerbils, 3 sessions per condition; Figure S4B) (two-way mixed model ANOVA; $F_{(1,2)} = 0.015$, $p = 0.91$). This suggests that perturbing the direct auditory cortex input into parietal cortex is unlike reducing auditory sensation. Together, our results reveal that HM4Di-mediated inhibition of auditory cortex projections into parietal cortex increases auditory integration time, demonstrating that parietal cortex integrates sensory input deriving directly from auditory cortex during this perceptual decision-making task.

Signal detection theory-based model can account for behavioral choices

Currently, our results suggest that parietal cortex integrates sensory inputs from auditory cortex to produce behavioral integration time. Here, we test whether the impairments to task performance from perturbing auditory cortex input into parietal cortex (Fig. 4E,F) and reducing parietal cortex activity (Fig. 3B,C) are due to elevated “noise” associated with the accumulation of sensory inputs. We utilized a signal-detection theory-based model to estimate the noise associated with each stimulus and its duration [48]. With this approach, a gerbil’s estimate of a given stimulus is modeled as a random variable drawn from a Gaussian distribution whose mean is equal to the true AM rate (4 or 10), and whose standard deviation is a free parameter (σ) estimated as the value that maximized the likelihood of the animal’s choices. On each trial, the animal’s predicted choice is generated by randomly selecting one variable from the Gaussian distribution that is then compared to a criterion, the mean of the two distributions (criterion = 7 Hz). If the randomly drawn variable is less than the criterion, the predicted choice is “choose left”, and if the randomly drawn variable is greater than the criterion, the predicted choice is “choose right” (Figure 5A). To account for improved performance with longer stimulus durations, the standard deviation of the sampled distribution was divided by the number of stimulus periods presented on each trial. A previous report showed that rats performing a visual accumulation of evidence task exhibited this particular noise scaling [48]. In order to evaluate the predicted choices of our signal-detection theory-based model, we performed 5-fold cross-validation and assessed the predictive power on held-out test sets. The model predicted the animal’s choices on held-out data for all stimulus durations (Figure 5B). This is represented by high goodness-of-fit values (r^2) across each animal (4 Hz trials: $r^2 = 0.91 \pm 0.02$; 10 Hz trials: $r^2 = 0.91 \pm 0.01$), as well as for pooled data across all animals (4 Hz trials: $r^2 = 0.97$; 10 Hz trials: $r^2 = 0.99$). Figure S5A displays model predictions under the assumption of independent noise (i.e., standard deviation divided by square root of the number of samples). We found that goodness-of-fit values were significantly worse under the assumption of independent noise compared with the assumption that noise grows linearly with the number of samples (Figure S5B; two-tailed t-test, 4 Hz trials: $p < 0.001$, $t = 6.30$; 10 Hz trials: $p < 0.001$, $t = 3.69$).

We compared σ values from the stimulus duration near minimum integration time values from “no drug” sessions (300 ms) across experimental groups to determine the effect of inactivating local parietal cortex activity (muscimol group) and perturbing auditory cortex inputs into parietal cortex (DREADDs group) on internal noise. We found a significant difference of σ values across experimental groups (non-parametric one-way ANOVA; 4 Hz trials: $X^2_{(3,35)} = 16.3$, $p = 0.001$; 10 Hz trials: $X^2_{(3,35)} = 13.96$, $p = 0.03$) (Figure 5C). Post-

hoc comparisons indicated that σ values were greatest among muscimol and DREADDs experimental groups (two-tailed t-tests; Holm-Bonferroni-corrected; 4Hz trials: muscimol versus no infusion: $p < 0.0001$, $t = 5.03$; muscimol versus saline: $p < 0.0001$, $t = 4.33$; DREADDs versus no infusion: $p = 0.003$, $t = 3.4$; DREADDs versus saline: $p = 0.01$, $t = 2.85$; 10 Hz trials: muscimol versus no infusion: $p = 0.002$, $t = 3.29$; muscimol versus saline: $p = 0.003$, $t = 3.41$; DREADDs versus no infusion: $p = 0.001$, $t = 3.42$; DREADDs versus saline: $p = 0.002$, $t = 3.47$). To determine whether experimental groups differed across non-sensory factors, such as attention or motivation, we included an explicit lapse rate parameter in the model, corresponding to stimulus-independent noise that would produce incorrect choices on the easiest trials. We found a significant difference in lapse rate across experimental groups (one-way ANOVA; $F_{(3,37)} = 7.79$, $p = 0.0004$) (Figure 5D), with the muscimol infusion group displaying the greatest lapse rates (post-hoc comparisons, two-tailed t-tests; Holm-Bonferroni-corrected; muscimol versus no infusion: $p = 0.0001$, $t = 3.5$; muscimol versus saline: $p < 0.0001$, $t = 3.6$; muscimol versus DREADDs: $p = 0.007$, $t = 2.7$). This suggests that parietal cortex inactivation produces a significant increase in errors at long stimulus durations compared to specifically inactivating auditory projections into parietal cortex, or that our muscimol activation was more pronounced than the DREADDs manipulation by inactivating a larger range of auditory-recipient input. Overall, these results suggest two mechanisms over which elevations in sensory noise impacts temporal integration task performance: 1) Reduced sensory input from auditory cortex to parietal cortex elevates sensory noise that increases integration time. 2) Reduced parietal cortex activity elevates sensory noise that increases integration time and also increases errors at long stimulus durations, which could be attributed to non-sensory impairments.

DISCUSSION

Parietal cortex activity is thought to play a role in the integration of noisy sensory information [32, 49, 50]. In fact, the extended timescale of noise correlations among parietal cortex neurons [51] could facilitate the accumulation of information projected from sensory cortices that drives perceptual judgements. Studies in non-human primates [12–14] and rodents [16, 24, 31] demonstrate that parietal cortex neurons are strongly modulated throughout the stimulus period, prior to the animal's decision. In the current study, we demonstrate that chemogenetically disrupting auditory cortex inputs into parietal cortex prolongs auditory accumulation of evidence (see Figure 4F), potentially due to increased sensory noise (Figure 5C). This suggests that disrupting sensory input into parietal cortex increases noise in the sensory representation, which extends the duration of time required for the accumulation of evidence that supports task performance. An increase in errors at long stimulus durations caused by direct parietal cortex inactivation with muscimol (Figure 3B) could suggest that accurate behavioral choices depend on the residual afferent and postsynaptic activity. For example, non-auditory inputs could be involved in the coordination and transformation of task-related sensory information into choice decisions and motor output [17, 52–54]. Furthermore, parietal cortex projects to the dorsal striatum and posterior secondary motor cortex, which are involved in biasing choice selection and motor control, respectively [55]. Therefore, inactivating parietal cortex would be expected to degrade

processing in these downstream regions that are necessary to produce appropriate behavioral responses.

The preservation of performance at long stimulus durations after deceasing neural activity suggests the involvement of separate pathways that contribute to this behavior. Auditory cortex has been causally implicated in many auditory tasks [56–59], and its downstream targets are many [60–62]. For example, the sensory striatum has been implicated in Left/Right motor actions [63]. Other possibilities include the frontal cortex where sensory information is transformed to more closely resemble behavioral relevance [64], the retrosplenial cortex which provides goal-directed spatial navigation trajectories [65], and secondary motor cortex which mediates planning and execution of motor actions [66]. With many areas downstream of auditory cortex involved in task performance, future studies could utilize a selective manipulation approach of anterogradely filling fibers within auditory cortex and implant cannulae or optical electrodes over an array of downstream targets to selectively perturb one or more of them, and determine their relative impact on behavioral performance.

A causal role for parietal cortex activity during sensory-guided task performance is currently uncertain. For example, while inactivation of parietal cortex impairs visual task performance, [24, 31, 67, 68] it has been suggested that this could be due to inactivation of adjacent secondary visual areas [34]. Other studies that inactivate parietal cortex show that auditory-guided performance is relatively unimpaired [15, 31, 68]. This is in contrast to our current results of impaired performance on an auditory discrimination task following chemogenetic perturbations of excitatory auditory cortex inputs to parietal cortex, as well as parietal cortex inactivation with muscimol. Both rats and gerbils possess similar cortical connectivity profiles such that parietal cortex in both species receives input from auditory cortex [21, 25, 60, 69, 70] (Figure 2), providing a pathway for the transmission of auditory information downstream primary auditory cortex. Thus, the difference in our results with previous reports of negligible effects of parietal cortex inactivation on an accumulation of evidence task with clicks [15, 31, 68] raises the possibility that our targeted auditory cortex recipient area of parietal cortex is distinct from the region of parietal cortex that was manipulated in previous studies. Specifically, previous reports did not contain anatomical anterograde or retrograde validation of auditory-recipient parietal cortex, and may not have targeted the centroid of the auditory cortex projections.

A second difference between our study and previous reports is the behavioral task structure. In previous studies, subjects were required to withhold their behavioral response until a “go” signal was presented. In contrast, our animals were permitted to respond as soon as possible following the stimulus presentation. Typically, our animals moved towards the reward tray prior to the end of the stimulus duration, comparable to reaction time accumulation of visual evidence tasks performed by non-human primates [12, 13]. This leaves open the possibility that withholding a choice decision, based on auditory cues in working memory, engages other pathways, thereby rendering the parietal cortex circuit unnecessary for the behavioral outcome. A third difference between our study and previous reports is the acoustic stimuli presented. Previous paradigms of auditory-based evidence accumulation tasks used clicks [15, 31, 68], whereas we presented amplitude-modulated broadband noise. Natural sounds

are composed of rich acoustic features such as modulations in sound intensity [71, 72]. In fact, auditory cortex activity synchronizes to slow modulation frequencies [73], where energy is concentrated for natural sounds such as speech and other communication sounds [36, 43]. Thus, it is possible that auditory cortex-recipient parietal cortex is preferentially activated by envelope information in the natural range, and subjects were better able to accumulate evidence from the slow AM stimuli that we used.

Across auditory behavioral paradigms, performance variability is often attributed to "internal noise." In fact, high internal noise is thought to limit efficient use of available acoustic cues, which accounts for poor behavioral performance in children [74, 75], following hearing loss [76], or with aging [77, 78]. In the current study, the deficits in decision-making behavior from perturbing parietal cortex activity could be due to elevated internal noise caused by reduced or perturbed sensory input. To examine this, we implemented a signal detection theory model that quantified the noise associated with each stimulus (σ parameter) (Figure 5A, B). Chemogenetically perturbing auditory cortex input into parietal cortex and inactivating parietal cortex with muscimol increased this noise parameter (Figure 5C). An important future direction would be to examine the dynamics of parietal cortex activity and determine how it accounts for or reflects internal noise.

STAR METHODS

RESOURCE AVAILABILITY

Lead Contact—Further information and requests for resources and reagents should be directed to and will be fulfilled by the Lead Contact, Justin Yao (jdyao@nyu.edu).

Materials Availability—This study did not generate new unique reagents.

Data and Code Availability: Behavioral source data and relevant MATLAB codes for generating figures are available at https://nyu.box.com/v/Yao-et-al-Current-Biology-2020.

EXPERIMENTAL MODEL AND SUBJECT DETAILS

Subjects—Mongolian gerbils (*Meriones unguiculatus*, N = 29, 14 males, 6–14 months old) were weaned from commercial breeding pairs (Charles River) and housed on a 12 h light/12 h dark cycle and were used for the psychophysics, chemogenetics, and pharmacological experiments. 9 gerbils were used for virus-mediated anatomical tracing experiments (Figure 2). All procedures were approved by the Institutional Animal Care and Use Committee at New York University.

METHOD DETAILS

Psychophysical testing

Behavioral Apparatus: Adult gerbils were placed in a plastic test cage in a sound-attenuating booth (Industrial Acoustics) and observed via a closed-circuit monitor. Acoustic stimuli were delivered from a calibrated free-field tweeter (DX25TG0504; Vifa) positioned 1 m above the test cage. Sound calibration measurements were made with a 1/4-inch free-field condenser recording microphone (Brüel & Kjaer) placed in the center of the cage.

Stimulus, food reward delivery, and behavioral data acquisition were controlled by a personal computer through custom MATLAB scripts (written by Dr. Daniel Stolzberg) and an RZ6 multifunction processor (Tucker-Davis Technologies).

Training: Behavioral measures of integration time were obtained using an appetitive one-interval two-alternative forced-choice (2AFC) procedure. Specifically, gerbils were placed on controlled food access and trained to discriminate between amplitude modulated (AM) frozen broadband noise (25-dB roll-off at 3.5 kHz and 20 kHz) at 4 versus 10 Hz at 100% modulation depth. Each 4 and 10 Hz AM stimulus were presented at a sound level of 66 dB SPL, had a 200 ms onset ramp, followed by an unmodulated period of 200 ms that transitions to an AM signal for a set duration, followed by an unmodulated period. The duration of the AM signal is defined as the stimulus duration. Animals were initially trained to initiate a trial by placing its nose in a cylindrical port for a minimum of 100 ms that interrupted an infrared beam, and to approach the appropriate left or right food tray when presented with the AM noise stimulus (4 Hz: left tray; 10 Hz: right tray). When a gerbil breaks the infrared beam at the correct food tray, a pellet dispenser (Med Associates) delivers one reward dustless precision pellet (20 mg; Bio-Serv). Once the gerbils are able to discriminate between 4 versus 10 Hz AM with a stimulus duration of 2000 ms (proportion of trials correct > 0.85) across two sessions, then shorter durations are added on subsequent sessions (e.g., 100, 300, 600, 800, and 1000 ms). For each trial, the probability of a 4 or 10 Hz AM stimulus presentation is 50% and its duration is a random draw. Figure 1A displays a schematic of the 2AFC AM discrimination task.

Testing: Perceptual sensitivity is assessed by presenting six durations for each of the 4 and 10 Hz AM stimuli (e.g., 100, 300, 600, 800, 1000, and 2000 ms). Correct trials occur when a gerbil approaches the appropriate food tray (4 Hz: left; 10 Hz: right). When a gerbil approaches the incorrect food tray, then a 2–4 sec timeout period is initiated during which the room light is switched off and the animal is unable to initiate a trial. If the gerbil does not approach either food tray within 5 sec of stimulus presentation, then the trial is aborted and scored as incorrect. Proportion correct is calculated by: Correct trials/Total # of trials. Response latency is calculated as the total duration following trial initiation (i.e., stimulus onset after placing nose in cylindrical port) until stimulus termination (i.e., breaks infrared beam at a chosen food tray).

Integration time is assessed by examining how performance scales with stimulus duration. Proportion of correct trials across stimulus durations for each AM rate will be fit with psychometric functions using the open-source package psignifit 4 for MATLAB [58, 79, 80]. Psychometric functions of the proportion of correct trials are plotted as a function of stimulus duration. Minimum integration time was defined as the stimulus duration at which proportion of correct trials = 0.76, which is equivalent to the signal detection metric, *d'*, equal to 1 [44, 45]. The maximum (steepest) slope between x-axis coordinates (stimulus duration) that bracketed the minimum integration time was assigned as the slope value. The analyses were performed on all behavior sessions where percent correct at 1000 and 2000 ms durations were ≥ 85%, and the animal performed ≥ 120 trials. The average number of

behavioral trials was 193 ± 5.42 trials per session. The total number of test sessions per animal was 3.

Viral injections of anatomical tracer—Gerbils were first anesthetized with isoflurane/O_2 and secured on a stereotaxic device (Kopf). The surgical scalp area was then shaved and cleaned with iodine and an incision was made to expose parietal, occipital, and frontal bones. For viral injections into parietal cortex, a craniotomy was made between 3.6–3.9 mm rostral and 2.5 mm lateral to lambda [46]. For viral injections into AC, the temporalis muscle was retracted and a craniotomy was made between 3.2–3.9 mm rostral to lambda and 1–1.5 mm ventral from the temporal ridge. A durotomy was performed over the region of interest and a glass pipette (Drummond) containing an anterograde (pAAV-hSyn-EGFP, Addgene plasmid 50465; pENN-AAV-hSyn-TurboRFP-WRPE-rBG, Addgene plasmid 105552) or retrograde tracer (pAAVrg-hSyn-EGFP, Addgene plasmid 50465) was attached to a microinjector (Nanoject). Two injections (200 nL) were made within each region of interest, first at 0.3 mm and then at 0.8 mm below the pial surface at an injection rate of 2 nL/sec. Following the injections, the exposed cortical surface was covered with a silicon elastomer (Kwik-Sil, World Precision Instruments) and the surgical incision was closed with sutures.

Cannula implantation surgery—Surgical procedures for cannula implantation were similar to those for viral injections. After exposing parietal, occipital, and frontal bones, bone screws were inserted into both frontal and occipital bones. Bilateral craniotomies were made along parietal bones between 3.6–3.9 mm rostral and 2.5 mm lateral to lambda. Double-guide cannulae (26 gauge, 3 mm cannula length, 0.5 mm center-to-center distance; C235GS-5–0.5/SPC; Plastics One) were angled 0 degrees in the mediolateral plane and placed above the cortical surface and secured with dental acrylic (Zimmer Biomet). The tip of the guides sat along the brain surface and dummy cannulae (extend 0.2 mm into cortex) were inserted to keep the guides clear and secured with aluminum dust caps. Following the placements of the cannulae, any exposed skull surface was covered with dental acrylic. Gerbils were given 7 days to recover before being placed on controlled food access prior to psychometric testing. After recovery, task motivation for each animal was monitored for a number of days (3–8 days, median = 4). Once animals surpassed the criterion of 120 trials, they began psychometric testing on the following day.

Cannula infusions—Cannula infusions were performed using previously described procedures [58]. Muscimol (Abcam) was dissolved in 0.9% NaCl to achieve a concentration of 4 mg/mL. Aliquots filled with 20 uL were stored at −20°C and used within 1 week. On the day of infusions, one aliquot was removed from the freezer, thawed to room temperature, and diluted to 1 mg/mL with 0.9% NaCl. Gerbils (n = 7) were anesthetized with isoflurane/O_2 and secured on a stereotaxic frame. Dust caps and dummy cannulae were removed from the guides. Double infusion cannulae (33 gauge, 3.5 mm cannula length, C235IS-5/SPC; Plastics One) were connected to PE-50 tubing (Plastics One), backfilled with mineral oil, and attached to glass syringes (10 μL, 1801 Gastight, Hamilton). Muscimol or saline was drawn into the tip of each cannula, and inserted into the guides that extend ~0.5 mm into parietal cortex. Bilateral infusions (0.2 uL/hemisphere, 0.2 uL/min) were

operated with a six-channel programmable pump (NE-1600, New Era). This entire process took ~10 min and animals recovered in their home cages for 30 min prior to behavioral testing.

Chemogenetic manipulation of auditory cortex to parietal cortex projections— We used a designer receptor exclusively activated by designer drugs (DREADDs) based method to perturb auditory cortex to parietal cortex projections. Well-trained gerbils (n = 5) were bilaterally injected with an adenovirus containing a CaMKII promotor that transfects pyramidal neurons with the inhibitory DREADDs receptor HM4Di (pAAV-CaMKIIa-hM4D(Gi)-mCherry, Addgene plasmid 50477) into auditory cortex. The surgical procedure was the same as described above for viral injections of anatomical tracers. Following injections, double guide cannulae were implanted above parietal cortex (see above). Once fully recovered, cannulae infusion procedures were conducted in all animals prior to psychometric testing. Specifically, prior to psychometric testing, compound 21 (C21; HelloBio; 5 mg/mL; 0.2 uL/hemisphere), a chemogenetic actuator of hM4D, or saline was drawn into the tip of the infusion cannulae and inserted into the guides that extend ~0.5 mm into parietal cortex.

Histology—At the termination of each experiment, animals were deeply anesthetized with sodium pentobarbital (150 mg/kg) and perfused with phosphate-buffered saline and 4% paraformaldehyde. Brains were extracted, post-fixed, sectioned (50–60 μm) on a vibratome (Leica), mounted on glass slides, and cover-slipped (Vectashield Antifade Mounting Medium with DAPI). Fluorescent imaging was conducted on a confocal microscope (Leica).

QUANTIFICATION AND STATISTICAL ANALYSIS

Signal detection theory model—To predict the gerbils' choices on each trial, we applied a signal detection theory-based model that estimated the width of the distribution of animals' internal estimates of the presented AM rates [48]. The model assumes that on each trial, a gerbil's percept of a presented stimulus is a noisy sample from a Gaussian distribution whose mean is the true AM rate, and whose standard deviation is a free parameter (σ). Thus, on a given trial, the animal's estimate of a presented AM rate stimulus (4 versus 10 Hz) is a random variable drawn from a Gaussian distribution whose mean is the AM rate associated with the presented stimulus (4 or 10), and whose standard deviation is a free parameter (σ). The randomly drawn variable is compared to a decision criterion, the mean of the two distributions (criterion = 7 Hz), and the sign predicts performance. If the randomly drawn variable is less than the criterion, the predicted choice is "choose left". If the randomly drawn variable is greater than the criterion, the predicted choice is "choose right" (Fig. 5A). Thus, on 4 Hz trials, correct responses occur when the randomly drawn variable is less than the criterion. On 10 Hz trials, correct responses occur when the randomly drawn variable is greater than the criterion. We also included an explicit lapse rate parameter, which corresponded to the fraction of trials on which the animals would guess (i.e., incorrect trials at very long stimulus durations), similar to other models of auditory accumulation of evidence in rodents [81]. We recognize that there are other potential ways of parameterizing the lapse rate, and an interesting future direction would be to explore these different parameterizations in more detail. For the purposes of the present manuscript, we

found that the additive/subtractive model provided a good fit to the data. The standard deviations for each distribution (σ_{4Hz} and σ_{10Hz}) and the lapse rate (lapse) were estimated as values that maximized the likelihood of the animals' choices, fitted with the Matlab function fmincon. To account for chronometric improvements in behavioral performance (i.e., improvements in task performance with longer stimulus duration), the noise of the sampled distributions on each trial were divided by the number of samples (i.e., 4 and 10 Hz modulations across a given stimulus duration) [48]. This was implemented by the following equations:

$$p(choose\ Right|10\ Hz) = \int_{crit}^{\infty} N\left(10, \sqrt{(\sigma_{10Hz}/samples)^2}\right)dx - lapse$$

$$p(choose\ Right|4\ Hz) = \int_{crit}^{\infty} N\left(4, \sqrt{(\sigma_{4Hz}/samples)^2}\right)dx + lapse$$

where *crit* is criterion, or 7 Hz. In order to evaluate the performance of the model, we performed 5-fold cross-validation and evaluated the predictive power of the model on the held-out test sets.

Statistical procedures—Statistical analyses and procedures were implemented in JMP 13.2.0 (SAS) or custom-written MATLAB scripts (The Mathworks) that incorporated the MATLAB Statistics Toolbox. Normally distributed data (as assessed by the Lilliefors test) are reported as mean ± SEM unless otherwise stated. When data were not normally distributed, non-parametric statistical tests were used when appropriate.

Supplementary Material

Refer to Web version on PubMed Central for supplementary material.

Acknowledgements

The work is supported by NIDCD F32DC016508 (JDY) and R01DC011284 (DHS)

Abbreviations

AC	core auditory cortex
AuD	secondary dorsal auditory area
AM	amplitude modulation
2AFC	two alternative forced choice
DREADDs	designer receptors exclusively activated by designer drugs
C21	compound 21

REFERENCES

1. Pandya PK, Rathbun DL, Moucha R, Engineer ND & Kilgard MP (2008). Spectral and temporal processing in rat posterior auditory cortex. Cereb Cortex 18, 301–314. [PubMed: 17615251]
2. Camalier CR, D'Angelo WR, Sterbing-D'Angelo SJ, de la Mothe LA & Hackett TA (2012). Neural latencies across auditory cortex of macaque support a dorsal stream supramodal timing advantage in primates. Proc Natl Acad Sci U S A 109, 18168–18173. [PubMed: 23074251]
3. Murray JD et al. (2014). A hierarchy of intrinsic timescales across primate cortex. Nat Neurosci 17, 1661–1663. [PubMed: 25383900]
4. Boemio A, Fromm S, Braun A & Poeppel D (2005). Hierarchical and asymmetric temporal sensitivity in human auditory cortices. Nat Neurosci 8, 389–395. [PubMed: 15723061]
5. Bendor D & Wang X (2007). Differential neural coding of acoustic flutter within primate auditory cortex. Nat Neurosci 10, 763–771. [PubMed: 17468752]
6. Scott BH, Malone BJ & Semple MN (2011). Transformation of temporal processing across auditory cortex of awake macaques. J Neurophysiol 105, 712–730. [PubMed: 21106896]
7. DeWitt I & Rauschecker JP (2012). Phoneme and word recognition in the auditory ventral stream. Proc Natl Acad Sci U S A 109, E505–14. [PubMed: 22308358]
8. de Heer WA, Huth AG, Griffiths TL, Gallant JL & Theunissen FE (2017). The Hierarchical Cortical Organization of Human Speech Processing. J Neurosci 37, 6539–6557. [PubMed: 28588065]
9. Fassihi A, Akrami A, Pulecchi F, Schönfelder V & Diamond ME (2017). Transformation of Perception from Sensory to Motor Cortex. Curr Biol 27, 1585–1596.e6. [PubMed: 28552362]
10. Shadlen MN & Kiani R (2013). Decision making as a window on cognition. Neuron 80, 791–806. [PubMed: 24183028]
11. Stine GM, Zylberberg A, Ditterich J & Shadlen MN (2020). Differentiating between integration and non-integration strategies in perceptual decision making. Elife 9.
12. Roitman JD & Shadlen MN (2002). Response of neurons in the lateral intraparietal area during a combined visual discrimination reaction time task. J Neurosci 22, 9475–9489. [PubMed: 12417672]
13. Huk AC & Shadlen MN (2005). Neural activity in macaque parietal cortex reflects temporal integration of visual motion signals during perceptual decision making. J Neurosci 25, 10420–10436. [PubMed: 16280581]
14. Kiani R, Hanks TD & Shadlen MN (2008). Bounded integration in parietal cortex underlies decisions even when viewing duration is dictated by the environment. J Neurosci 28, 3017–3029. [PubMed: 18354005]
15. Erlich JC, Brunton BW, Duan CA, Hanks TD & Brody CD (2015). Distinct effects of prefrontal and parietal cortex inactivations on an accumulation of evidence task in the rat. Elife 4.
16. Hanks TD, Kopec CD, Brunton BW, Duan CA, Elrich JC, & Brody CD (2015). Distinct relationships of parietal and prefrontal cortices to evidence accumulation. Nature 520, 220–223. [PubMed: 25600270]
17. Zhou Y & Freedman DJ (2019). Posterior parietal cortex plays a causal role in perceptual and categorical decisions. Science 365, 180–185. [PubMed: 31296771]
18. Pandya DN & Kuypers HG (1969). Cortico-cortical connections in the rhesus monkey. Brain Res 13, 13–36. [PubMed: 4185124]
19. Divac I, Lavail JH, Rakic P & Winston KR (1977). Heterogeneous afferents to the inferior parietal lobule of the rhesus monkey revealed by the retrograde transport method. Brain Res 123, 197–207. [PubMed: 402983]
20. Hyvärinen J (1982). Posterior parietal lobe of the primate brain. Physiol Rev 62, 1060–1129. [PubMed: 6806834]
21. Reep RL, Chandler HC, King V & Corwin JV (1994). Rat posterior parietal cortex: topography of corticocortical and thalamic connections. Exp Brain Res 100, 67–84. [PubMed: 7813654]
22. Lewis JW & Van Essen DC (2000). Mapping of architectonic subdivisions in the macaque monkey, with emphasis on parieto-occipital cortex. J Comp Neurol 428, 79–111. [PubMed: 11058226]

23. Rauschecker JP & Scott SK (2016). Maps and streams in the auditory cortex: nonhuman primates illuminate human speech processing. Nat Neurosci 535, 285–288.
24. Harvey CD, Coen P & Tank DW (2012). Choice-specific sequences in parietal cortex during a virtual-navigation decision task. Nature 484, 62–68. [PubMed: 22419153]
25. Wilber AA, Clark BJ, Demecha AJ, Mesina L, Vos JM, & McNaughton BL (2014). Cortical connectivity maps reveal anatomically distinct areas in the parietal cortex of the rat. Front Neural Circuits 8, 146. [PubMed: 25601828]
26. Hackett TA, de la Mothe LA, Camalier CR, Falchier A, Lakatos P, Kajikawa Y, & Schroeder CE (2014). Feedforward and feedback projections of caudal belt and parabelt areas of auditory cortex: refining the hierarchical model. Front Neurosci 8, 72. [PubMed: 24795550]
27. Song YH, Kim JH, Jeong HW, Choi I, Jeong D, Kim K, & Lee SH (2017). A Neural Circuit for Auditory Dominance over Visual Perception. Neuron 93, 1236–1237.
28. Stricanne B, Andersen RA & Mazzoni P (1996). Eye-centered, head-centered, and intermediate coding of remembered sound locations in area LIP. J Neurophysiol 76, 2071–2076. [PubMed: 8890315]
29. Nakamura K (1999). Auditory spatial discriminatory and mnemonic neurons in rat posterior parietal cortex. J Neurophysiol 82, 2503–2517. [PubMed: 10561422]
30. Linden JF, Grunewald A & Andersen RA (1999). Responses to auditory stimuli in macaque lateral intraparietal area. II. Behavioral modulation. J Neurophysiol 82, 343–358. [PubMed: 10400963]
31. Raposo D, Kaufman MT & Churchland AK (2014). A category-free neural population supports evolving demands during decision-making. Nat Neurosci 17, 1784–1792. [PubMed: 25383902]
32. Hanks TD, Ditterich J & Shadlen MN (2006). Microstimulation of macaque area LIP affects decision-making in a motion discrimination task. Nat Neurosci 9, 682–689. [PubMed: 16604069]
33. Katz LN, Yates JL, Pillow JW & Huk AC (2016). Dissociated functional significance of decision-related activity in the primate dorsal stream. Nature 535, 285–288. [PubMed: 27376476]
34. Brody CD & Hanks TD (2016). Neural underpinnings of the evidence accumulator. Curr Opin Neurobiol 37, 149–157. [PubMed: 26878969]
35. Shannon RV, Zeng FG, Kamath V, Wygonski J & Ekelid M (1995). Speech recognition with primarily temporal cues. Science 270, 303–304. [PubMed: 7569981]
36. Singh NC & Theunissen FE (2003). Modulation spectra of natural sounds and ethological theories of auditory processing. J Acoust Soc Am 114, 3394–3411. [PubMed: 14714819]
37. Oganian Y & Chang EF (2019). A speech envelope landmark for syllable encoding in human superior temporal gyrus. Sci Adv 5, eaay6279. [PubMed: 31976369]
38. Viemeister NF (1979). Temporal modulation transfer functions based upon modulation thresholds. J Acoust Soc Am 66, 1364–1380. [PubMed: 500975]
39. Sheft S & Yost WA (1990). Temporal integration in amplitude modulation detection. J Acoust Soc Am 88, 796–805. [PubMed: 2212305]
40. Lee J (1994). Amplitude modulation rate discrimination with sinusoidal carriers. J Acoust Soc Am 96, 2140–2147. [PubMed: 7963027]
41. Eddins EA & Green DM (1995). In Hearing (Academic Press, Inc.), pp. 207–242.
42. Lee J & Bacon SP (1997). Amplitude modulation depth discrimination of a sinusoidal carrier: effect of stimulus duration. J Acoust Soc Am 101, 3688–3693. [PubMed: 9193056]
43. Ding N, Patel AD, Chen L, Butler H, Luo C, & Poeppel D (2017). Temporal modulations in speech and music. Neurosci Biobehav Rev 81, 181–187. [PubMed: 28212857]
44. DM G & JA S (1966). Signal Detection Theory and Psychophysics (New York: Wiley).
45. Hacker MJ & Ratcliff R (1979). A revised table of d′ for M-alternative forced choice. Perception & Psychophysics, 26, 168–170.
46. Radtke-Schuller S, Schuller G, Angenstein F, Grosser OS, Goldschmidt J, & Budinger E (2016). Brain atlas of the Mongolian gerbil (Meriones unguiculatus) in CT/MRI-aided stereotaxic coordinates. Brain Struct Funct 221 Suppl 1, 1–272.
47. Hromádka T, DeWeese MR & Zador AM (2008). Sparse representation of sounds in the unanesthetized auditory cortex. PLoS biology 6.

48. Scott BB, Constantinople CM, Erlich JC, Tank DW & Brody CD (2015). Sources of noise during accumulation of evidence in unrestrained and voluntarily head-restrained rats. Elife 4, e11308. [PubMed: 26673896]
49. Shadlen MN & Newsome WT (2001). Neural basis of a perceptual decision in the parietal cortex (area LIP) of the rhesus monkey. J Neurophysiol 86, 1916–1936. [PubMed: 11600651]
50. Gold JI & Shadlen MN (2007). The neural basis of decision making. Annu Rev Neurosci 30, 535–574. [PubMed: 17600525]
51. Runyan CA, Piasini E, Panzeri S & Harvey CD (2017). Distinct timescales of population coding across cortex. Nature 548, 92–96. [PubMed: 28723889]
52. Williams ZM, Elfar JC, Eskandar EN, Toth LJ & Assad JA (2003). Parietal activity and the perceived direction of ambiguous apparent motion. Nat Neurosci 6, 616–623. [PubMed: 12730699]
53. Freedman DJ & Assad JA (2016). Neuronal Mechanisms of Visual Categorization: An Abstract View on Decision Making. Annu Rev Neurosci 39, 129–147. [PubMed: 27070552]
54. Ibos G & Freedman DJ (2017). Sequential sensory and decision processing in posterior parietal cortex. Elife 6.
55. Hwang EJ, Dahlen JE, Mukundan M & Komiyama T (2017). History-based action selection bias in posterior parietal cortex. Nat Commun 8, 1242. [PubMed: 29089500]
56. Ohl A, Schröder K, Keller D, Meyer-Plath A, Bienert H, Husen B, & Rune GM (1999). Chemical micropatterning of polymeric cell culture substrates using low-pressure hydrogen gas discharge plasmas. J Mater Sci Mater Med 10, 747–754. [PubMed: 15347945]
57. Tsunada J, Liu AS, Gold JI & Cohen YE (2016). Causal contribution of primate auditory cortex to auditory perceptual decision-making. Nat Neurosci 19, 135–142. [PubMed: 26656644]
58. Caras ML & Sanes DH (2017). Top-down modulation of sensory cortex gates perceptual learning. Proc Natl Acad Sci U S A 114, 9972–9977. [PubMed: 28847938]
59. Ceballo S, Piwkowska Z, Bourg J, Daret A & Bathellier B (2019). Targeted Cortical Manipulation of Auditory Perception. Neuron 104, 1168–1179.e5. [PubMed: 31727548]
60. Budinger E, Laszcz A, Lison H, Scheich H & Ohl FW (2008). Non-sensory cortical and subcortical connections of the primary auditory cortex in Mongolian gerbils: bottom-up and top-down processing of neuronal information via field AI. Brain Res 1220, 2–32. [PubMed: 17964556]
61. Budinger E & Scheich H (2009). Anatomical connections suitable for the direct processing of neuronal information of different modalities via the rodent primary auditory cortex. Hear Res 258, 16–27. [PubMed: 19446016]
62. Hackett TA (2011). Information flow in the auditory cortical network. Hear Res 271, 133–146. [PubMed: 20116421]
63. Znamenskiy P & Zador AM (2013). Corticostriatal neurons in auditory cortex drive decisions during auditory discrimination. Nature 497, 482–485. [PubMed: 23636333]
64. Fritz JB, David SV, Radtke-Schuller S, Yin P & Shamma SA (2010). Adaptive, behaviorally gated, persistent encoding of task-relevant auditory information in ferret frontal cortex. Nat Neurosci 13, 1011–1019. [PubMed: 20622871]
65. Vedder LC, Miller AMP, Harrison MB & Smith DM (2017). Retrosplenial Cortical Neurons Encode Navigational Cues, Trajectories and Reward Locations During Goal Directed Navigation. Cereb Cortex 27, 3713–3723. [PubMed: 27473323]
66. Olson JM, Li JK, Montgomery SE & Nitz DA (2020). Secondary Motor Cortex Transforms Spatial Information into Planned Action during Navigation. Curr Biol. 30, 1–10. [PubMed: 31839447]
67. Goard MJ, Pho GN, Woodson J & Sur M (2016). Distinct roles of visual, parietal, and frontal motor cortices in memory-guided sensorimotor decisions. Elife 5, e13764. [PubMed: 27490481]
68. Licata AM, Kaufman MT, Raposo D, Ryan MB, Sheppard JP, & Churchland AK (2017). Posterior parietal cortex guides visual decisions in rats. Journal of Neuroscience 37, 4954–4966. [PubMed: 28408414]
69. Kolb B & Walkey J (1987). Behavioural and anatomical studies of the posterior parietal cortex in the rat. Behav Brain Res 23, 127–145. [PubMed: 3566907]

70. Budinger E, Heil P, Hess A & Scheich H (2006). Multisensory processing via early cortical stages: connections of the primary auditory cortical field with other sensory systems. Neuroscience 143, 1065–1083. [PubMed: 17027173]

71. McDermott JH & Simoncelli EP (2011). Sound texture perception via statistics of the auditory periphery: evidence from sound synthesis. Neuron 71, 926–940. [PubMed: 21903084]

72. Młynarski W & McDermott JH (2019). Ecological origins of perceptual grouping principles in the auditory system. Proc Natl Acad Sci U S A 116, 25355–25364. [PubMed: 31754035]

73. Peelle JE & Davis MH (2012). Neural Oscillations Carry Speech Rhythm through to Comprehension. Front Psychol 3, 320. [PubMed: 22973251]

74. Buss E, Hall III JW & Grose JH (2006). Development and the role of internal noise in detection and discrimination thresholds with narrow band stimuli. The Journal of the Acoustical Society of America 120, 2777–2788. [PubMed: 17139738]

75. Cabrera L, Varnet L, Buss E, Rosen S & Lorenzi C (2019). Development of temporal auditory processing in childhood: Changes in efficiency rather than temporal-modulation selectivity. The Journal of the Acoustical Society of America 146, 2415–2429. [PubMed: 31672005]

76. Wallaert N, Moore BCJ, Ewert SD & Lorenzi C (2017). Sensorineural hearing loss enhances auditory sensitivity and temporal integration for amplitude modulation. The Journal of the Acoustical Society of America 141, 971–980. [PubMed: 28253641]

77. Schneider BA, Daneman M & Pichora-Fuller MK (2002). Listening in aging adults: from discourse comprehension to psychoacoustics. Canadian Journal of Experimental Psychology/Revue canadienne de psychologie expérimentale 56, 139. [PubMed: 12271745]

78. Gilbertson L, Lutfi RA & Lee J (2015). Estimates of decision weights and internal noise in the masked discrimination of vowels by young and elderly adults. The Journal of the Acoustical Society of America 137, EL403–EL407. [PubMed: 26093447]

79. Schütt HH, Harmeling S, Macke JH & Wichmann FA (2016). Painfree and accurate Bayesian estimation of psychometric functions for (potentially) overdispersed data. Vision Res 122, 105–123. [PubMed: 27013261]

80. Yao JD & Sanes DH (2018). Developmental deprivation-induced perceptual and cortical processing deficits in awake-behaving animals. Elife 7.

81. Brunton BW, Botvinick MM & Brody CD Rats and humans can optimally accumulate evidence for decision-making. Science 340, 95–98 (2013). [PubMed: 23559254]

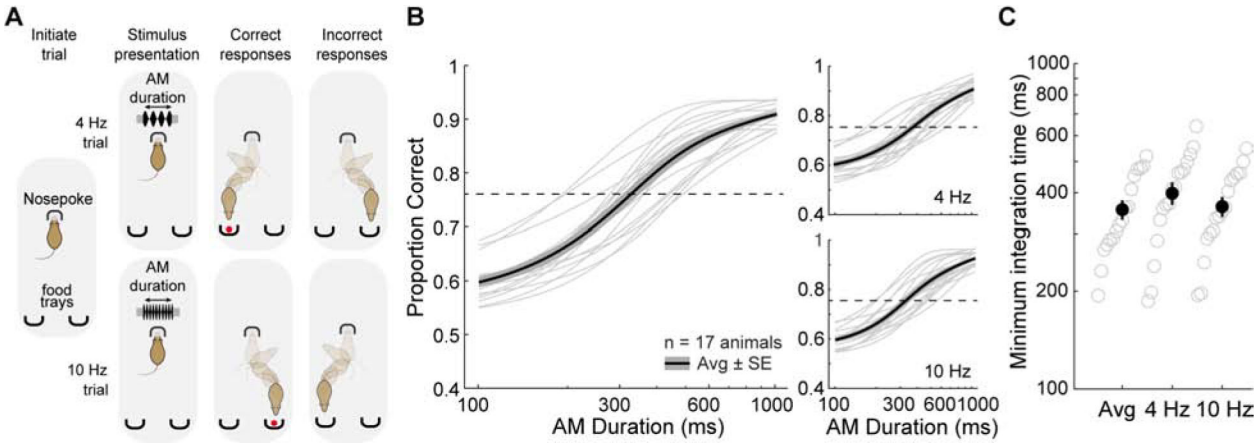

Figure 1. Behavioral measures of auditory integration time.

A) Schematic of the auditory integration task, a two-alternative forced choice AM noise discrimination task. Gerbils are required to discriminate between AM noise at 4 versus 10 Hz across a range of stimulus durations (100–2000 ms). B) Psychometric functions from the average of all animals (thin lines). Thick lines represent the overall average across all animals and the shaded region represents average ± SE. C) Distribution of calculated minimum integration times from each animal across separate trial types. See also Figure S1.

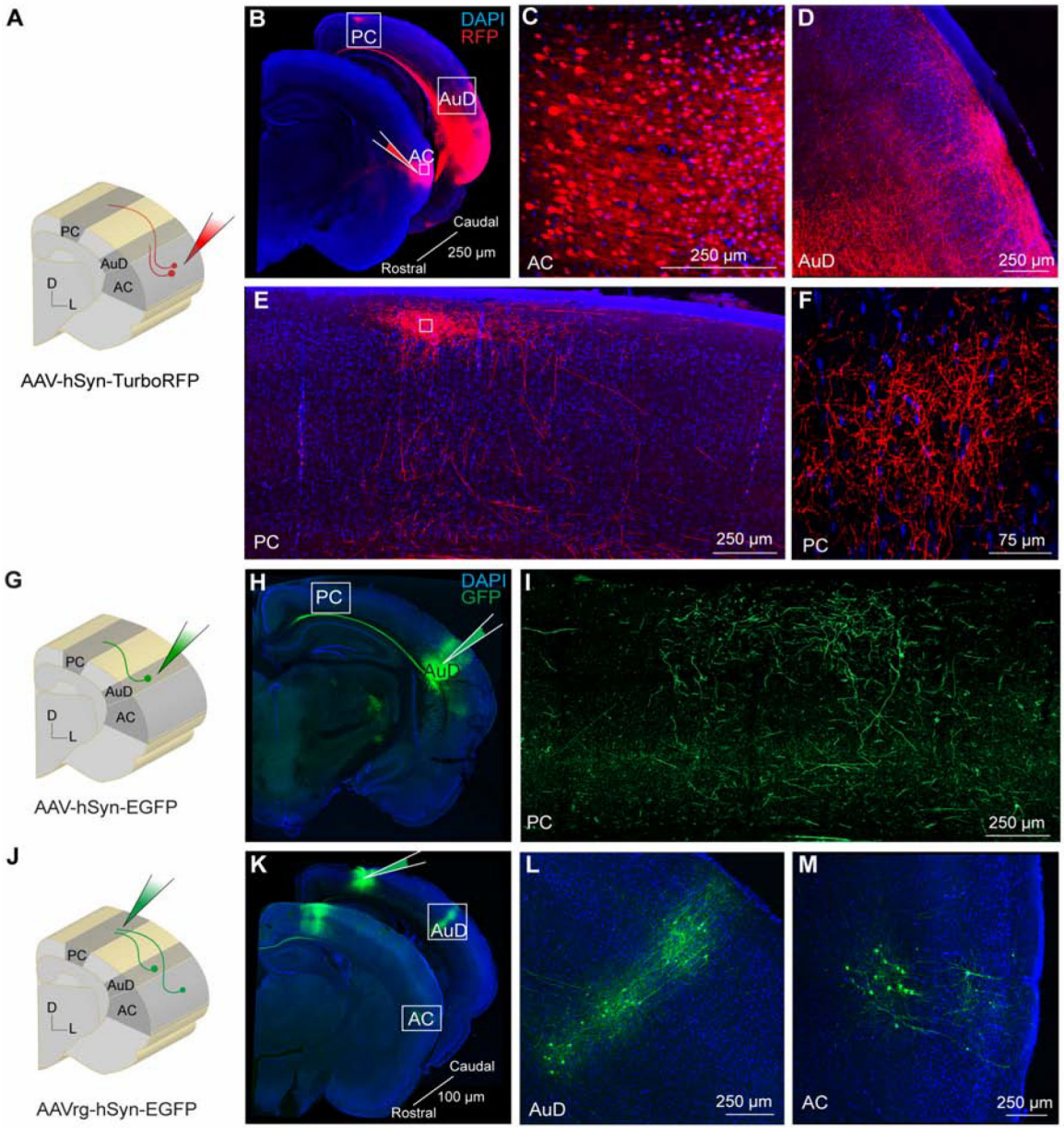

Figure 2. Auditory cortical neurons project to the parietal cortex.

A) Schematic diagram showing auditory cortex site of anterograde AAV-hSyn-TurboRFP injection. B) Brain slices showing the injection site in auditory cortex and anterograde labeling in secondary dorsal auditory area and parietal cortex. C) Expanded inset of auditory cortex showing high-magnification of labeled cell bodies within the injection site. D) Expanded inset of secondary dorsal auditory area showing dense axonal labeling. E) Expanded inset of parietal cortex showing dense axonal labeling. F) Expanded inset of parietal cortex at higher magnification. G) Schematic diagram showing secondary dorsal auditory area site of anterograde AAV-hSyn-EGFP injection. H) Brain slice showing the injection site in secondary dorsal auditory area. I) Expanded inset showing high-magnification of axonal labeling in parietal cortex. J) Schematic diagram showing parietal

cortex site of retrograde AAV-hSyn-EGFP injection. K) Brain slices showing the injection site in parietal cortex and retrograde labeling in secondary dorsal auditory area and auditory cortex. L) Expanded inset of secondary dorsal auditory area showing cell body labeling. M) Expanded inset of auditory cortex showing cell body labeling. Core auditory cortex (AC), secondary dorsal auditory area (AuD), parietal cortex (PC).

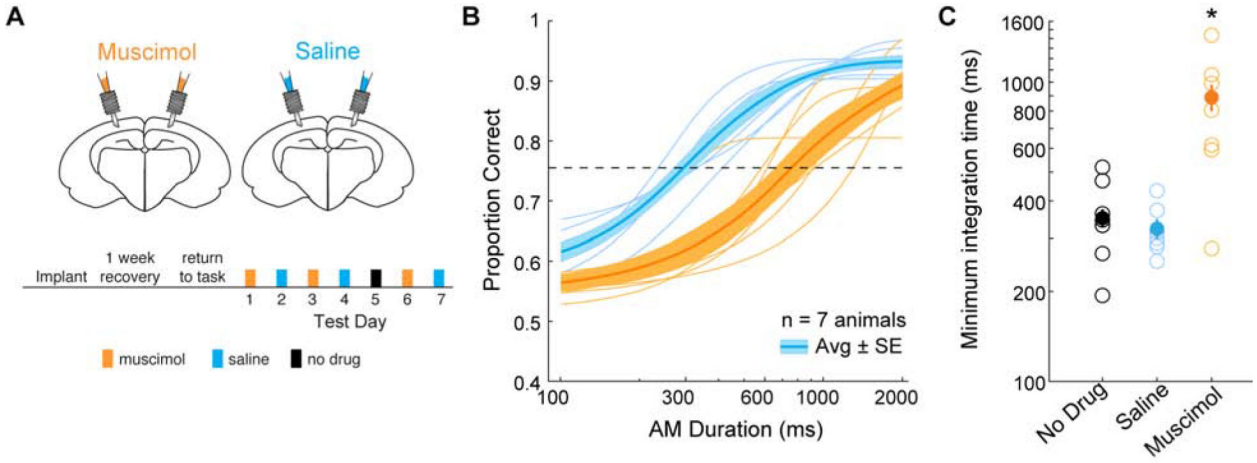

Figure 3. Inactivation of parietal cortex increases auditory integration time.

A) Schematic of cannula implant over parietal cortex and timeline of experimental test sessions. Infusions of muscimol and saline into parietal cortex alternated across test session days. Prior to the last muscimol test session, neither muscimol or saline were infused. B) Average psychometric functions across all animals (thick lines) and average psychometric functions from each animal during muscimol (orange) and saline (blue) infusion sessions (thin lines). The shaded regions represent average ± SE. See text for statistical comparisons. C) Distribution of calculated minimum integration times from each animal as a function of infusion condition. Post-hoc analyses revealed minimum integration times under muscimol (orange) were significantly different from no drug (black) (two-tailed t-test; Holm-Bonferroni-corrected; $p = 0.02$, $t = 3.02$) and saline (blue) (two-tailed t-test; Holm-Bonferroni-corrected; $p = 0.01$, $t = 3.48$) sessions. See also Figure S2.

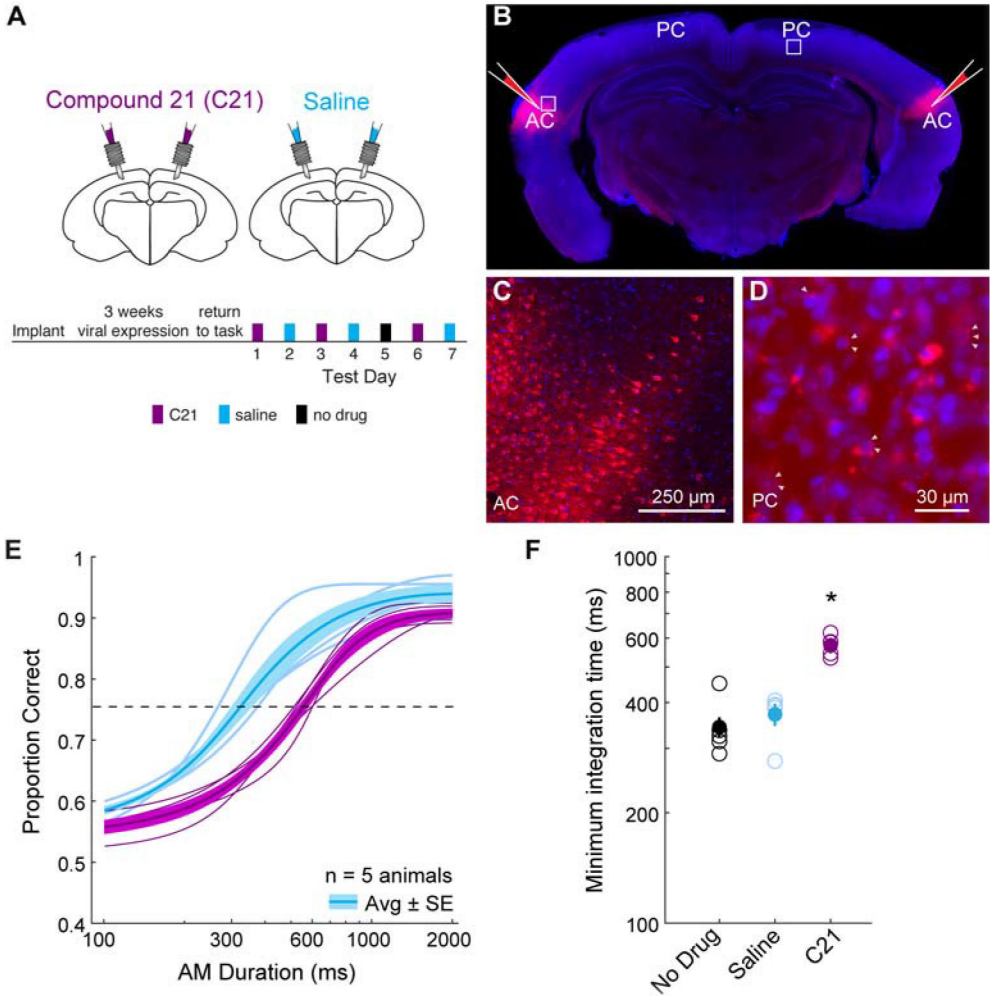

Figure 4. Perturbing auditory cortex inputs into parietal cortex increases auditory integration time.

A) Schematic of cannula implant over parietal cortex and timeline of experimental test sessions. Infusions of C21 and saline into parietal cortex alternated across test session days. B) Brain slice showing bilateral injections of pAAV-CaMKIIa-hM4D(Gi)-mCherry into auditory cortex. C) High magnification of expanded inset near auditory cortex injection site with labeled cell bodies. D) High magnification of expanded inset in parietal cortex confirms perisomatic labeling (white triangles) from injection sites in B. E) Average psychometric functions across all animals (thick lines) and average psychometric functions from each animal during C21 (purple) and saline (blue) infusion sessions (thin lines). See text for statistical comparisons. F) Distribution of calculated minimum integration times from each animal as a function of infusion condition. Post-hoc analyses revealed minimum integration times under C21 (purple) were significantly different from no drug (black) (two-tailed t-test; Holm-Bonferroni-corrected; $p = 0.005$, $t = 5.61$) and saline (blue) (two-tailed t-test; Holm-Bonferroni-corrected; $p = 0.003$, $t = 6.65$) sessions. Core auditory cortex (AC), parietal cortex (PC). See also Figure S3 and Figure S4.

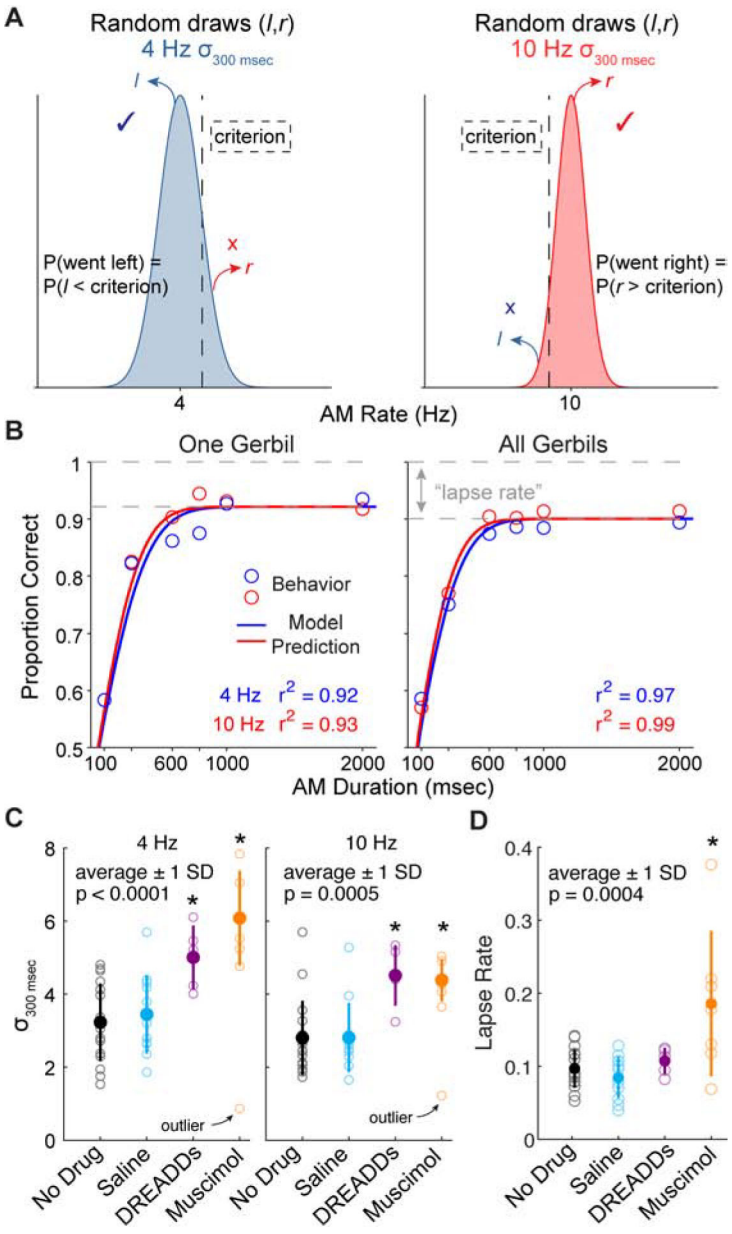

Figure 5. Signal detection theory-based model predicts animal's choices.

A) The model assumes that on each trial, a random variable is selected from the corresponding distribution (4 or 10 Hz) and is compared to a criterion (vertical dashed line). The mean of each Gaussian distribution is equal to each AM rate (4 and 10) and the standard deviation (σ) is a free parameter that was fit to the behavioral data using maximum likelihood estimation. The choice is determined by whether the selected random variable is less than or greater than the criterion (vertical dashed line) (left choice if < criterion; right choice if > criterion). B) Comparison of the behavioral data (symbols) with model predictions (lines) for held-out data (5-fold cross validation) from one animal (left) and all animals (right). Goodness of fit between behavioral data and model predictions are represented by r^2 values. C) σ values from the stimulus duration of 300 msec across each test condition. Outlier points were excluded in the statistical tests. D) Lapse rate across each

test condition. See text for statistical comparisons. Error bars represent ± 1 standard deviation. See also Figure S5.

KEY RESOURCES TABLE

REAGENT or RESOURCE	**SOURCE**	**IDENTIFIER**
Bacterial and Virus Strains		
pAAV-hSyn-EGFP	Addgene	RRID:Addgene_50465
pENN-AAV-hSyn-TurboRFP-WRPE-rBG	Addgene	Cat # 105552-AAV1
pAAVrg-hSyn-EGFP	Addgene	Cat # 50465-AAVrg
pAAV-CaMKIIa-hM4D(Gi)-mCherry	Addgene	RRID:Addgene_50477
Chemicals, Peptides, and Recombinant Proteins		
VectaShield with DAPI	Vector Labs	RRID: AB_2336790
Muscimol	Abcam	Cat # ab120094
Compound 21	HelloBio	Cat # HB6124
Experimental Models: Organisms/Strains		
Gerbil (*Meriones unguiculatus)*	Charles River Laboratories	https://www.criver.com
Software and Algorithms		
MATLAB	Mathworks	https://www.mathworks.com/
Adobe illustrator 2019	Adobe Systems	https://www.adobe.com/
Deposited Data		
All data	This paper	https://nyu.box.com/v/Yao-et-al-Current-Biology-2020